Turkish Journal of Electrical Engineering & Computer Sciences

http://journals.tubitak.gov.tr/elektrik/

Research Article

Turk J Elec Eng & Comp Sci
(2018) 26: 743 – 754

doi:10.3906/elk-1706-250

A novel solution in the simultaneous deep optimization of RGB-D camera calibration parameters using metaheuristic algorithms

Amir SAFAEI[1], **Saeid FAZLI**[2,*]
[1]Department of Electrical Engineering, Faculty of Engineering, University of Zanjan, Zanjan, Iran
[2]Research Institute of Modern Biological Techniques, University of Zanjan, Zanjan, Iran

Received: 21.06.2017 • **Accepted/Published Online:** 15.11.2017 • **Final Version:** 30.03.2018

Abstract: This article presents a novel method for estimating 19 parameters of RGB and depth camera calibration simultaneously. The proposed algorithm is based on applying metaheuristic methods for deep optimization and estimating all parameters of intrinsic, extrinsic, and lens distortions of cameras. This paper compares four metaheuristic algorithms, i.e. a genetic algorithm, particle swarm optimization, the colonial competitive algorithm, and the shuffled frog leaping algorithm, with a numerical algorithm called singular value decomposition. The proposed method does not need the initial estimation for optimization and it can avoid being trapped in local minima. By using nondirect estimation, we achieve middle computing matrices such as the homography matrix, which is used in the pinhole camera model. Both versions of Kinect sensors are used for the experimental evaluation. The mean square of the reprojection error criteria is defined as the objective function in the proposed algorithm. The experimental results show that the proposed method is more efficient and accurate than traditional numerical solutions.

Key words: Colonial competitive algorithm, homography, Kinect calibration, metaheuristic algorithm, radial lens distortion, shuffled frog leaping algorithm

1. Introduction

The aim of camera calibration is the extraction of intrinsic and extrinsic parameters and the estimation of radial and tangential lens distortions. In a calibration problem, the usage of projection equations should relate 3D world coordinates to 2D image coordinates. This projection in a pinhole camera is modeled by the homography matrix. Many methods have been proposed for camera calibration and the selection criteria depend on environmental parameters, accuracy, and equipment. We used a simple plane grid of a checkerboard based on the Zhang method [1] that is observed in at least three orientations. In this method, the homography matrix should be estimated and it would be the base matrix for the subsequent steps of finding intrinsic and extrinsic parameters. The traditional literature uses the least-square method for solving equations. Owing to the statistical bias of this method [2,3], Kanatani proposed a renormalized maximum likelihood estimation [4].

Evolutionary algorithms have been proposed for solving calibration equations. The selection of these methods depends on the essence of the equations. In the calibration problem, both local and global searches are important, and this paper proposes a comparative solution through metaheuristic and numerical methods.

In the Zhang method [1], the Levenberg–Marquardt algorithm for solving equations was proposed. This algorithm searches for a local minimum and not necessarily a global one. Hartley et al. [5] proposed a

*Correspondence: fazli@znu.ac.ir

noniterative method called direct linear transformation. This method uses the total least squares computation of the linear system of equations. Harker et al. [6] proposed a new noniterative solution based on the error structure of the estimation matrix. They combined the forward H and reverse G projections to eliminate the systematic bias of estimation. Herrera et al. [7] proposed a new technique for the simultaneous calibration of two color cameras, with conjunction of a depth camera, and the relative pose between them. They used Kinect as a depth sensor. Raposo et al. [8] improved the method of Herrera et al. [7] by decreasing the number of images in the dataset (about 6–10 image-disparity pairs of the model plane). They also used the Kinect sensor for the experiment and compared their results with the two versions of the Herrera method. Ji et al. [9] used a genetic algorithm (GA) for camera calibration and proved that their method works with a minimum number of control points. They showed that the GA method does not need an initial guess and their results were improved in convergence, accuracy, and robustness. Another GA method, proposed by Hati et al. [10], determines two rotational and three translational parameters. Song et al. [11] used particle swarm optimization (PSO) on synthetic and real images for camera calibration. They used 35 sample points on the calibration box but assumed that the cell shape of the CCD camera is square; therefore, the skewness of the intrinsic matrix was assumed to be zero. Merras et al. [12] proposed an improved GA for camera calibration with varying parameters. They compared their results with Tsai's [13] method on synthetic and real data. Yilmaz et al. [14] proposed external calibration parameters between stereo and Kinect sensors and used these parameters to compensate for misalignments in 3D reconstruction. A thorough survey on the Kinect sensor was presented by Han et al. [15].

In this paper, we use iterative metaheuristic methods for the estimation of all camera calibration parameters. The simulation of the proposed method has been accomplished on the Zhang dataset [1]. This dataset provides a text file with each image to test the efficiency of the calibration algorithm independently of the corner detection method that is applied in checkerboard images. In the next section, modeling between the 3D world plane and its projected 2D image with the extraction of intrinsic, extrinsic, and lens distortions is discussed. Section 3 describes the proposed method. In Section 4, the simulation results are shown and analyzed. In Section 5, the experimental results with both versions of Kinect sensors are discussed and the undistortion of the captured images is shown. Finally, the conclusion of this research is presented.

2. Projection of model plane into image plane

Based on the calibration object, the camera calibration can be divided into three groups: 3D reference objects, 2D plane-based objects, and 1D line objects. Other methods such as self-calibration, vanishing points for orthogonal directions, and calibration from pure rotation have been suggested in some papers [16]. In this paper, we use the second category for the calibration procedure and the modeling of projection is described as follows.

2.1. Plane projection

A 3D point in world coordinates or the coordinate system of the scene (CSS), its correspondence in the camera coordinate system (CCS), and its 2D projection in the image plane is denoted by $M=[X,Y,Z]^T$, $M_C=[X_C,Y_C,Z_C]^T$, and $m=[u,v]^T$, respectively. Based on the Zhang method [1], a 2D plane-based object is used, and by assuming $Z=0$ for the model plane in the 3D world coordinates, we have $M=[X,Y,0]^T$. By adding a one as the last row of each vector, we show the augmented vectors as:

$$\tilde{M} = [X, Y, 0, 1]^T, \tag{1}$$

$$\tilde{m} = [u, v, 1]^T. \tag{2}$$

As shown in Figure 1, from the pinhole camera model, the projection of the 3D point to the image plane is given by:

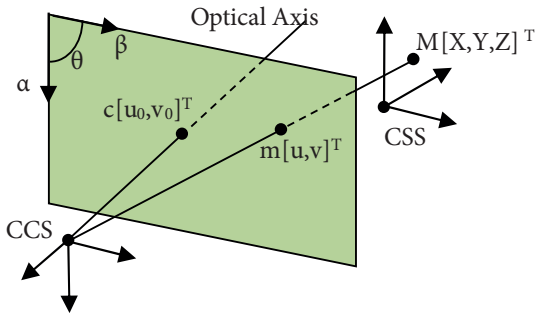

Figure 1. Pinhole camera model.

$$s\tilde{m} = A[R \quad t]\tilde{M}, \tag{3}$$

where s is an arbitrary scaling factor, A is the camera intrinsic matrix, R and t are respectively the rotation and translation matrices, and the combination of $[R\ t]$ gives the extrinsic matrix. If $[\ r_1 \quad r_2 \quad r_3\ ]$ denotes the columns of the rotation matrix R, because of Z=0 we can rewrite Eq. (3) as follows:

$$s\tilde{m} = A[\ r_1 \quad r_2 \quad r_3 \quad t\ ] \begin{bmatrix} X \\ Y \\ 0 \\ 1 \end{bmatrix} = A[\ r_1 \quad r_2 \quad t\ ] \begin{bmatrix} X \\ Y \\ 1 \end{bmatrix}. \tag{4}$$

The model point M and its projection point m can be related to each other by:

$$s\tilde{m} = H\tilde{M}, \tag{5}$$

where $H = A[\ r_1 \quad r_2 \quad t\ ]$ is a 3×3 matrix called the homography matrix, and, since Z=0, the model point is shown by $\tilde{M} = [X, Y, 1]^T$.

2.2. Orthonormality of the homography matrix

By denoting the columns of the homography matrix as $[\ h_1 \quad h_2 \quad h_3\ ]$, we have:

$$[\ h_1 \quad h_2 \quad h_3\ ] = \lambda A[\ r_1 \quad r_2 \quad t\ ], \tag{6}$$

where λ is an arbitrary scalar. Because of the orthonormality of r_1 and r_2, $\langle r_1, r_2 \rangle = 0$ and $\langle r_1, r_1 \rangle = \langle r_2, r_2 \rangle$:

$$\begin{aligned} h_1^T (A^{-1})^T A^{-1} h_2 &= 0 \\ h_1^T (A^{-1})^T A^{-1} h_1 &= h_2^T (A^{-1})^T A^{-1} h_2 \end{aligned}. \tag{7}$$

Before solving Eq. (7), determining the homography elements is essential.

2.3. Extraction of equations system

Using Eq. (5), expanding the matrix format, we have:

$$u = \frac{h_{11}X + h_{12}Y + h_{13}}{h_{31}X + h_{32}Y + h_{33}}, v = \frac{h_{21}X + h_{22}Y + h_{23}}{h_{31}X + h_{32}Y + h_{33}}, s = h_{31}X + h_{32}Y + h_{33}. \tag{8}$$

Rewriting this in the matrix format:

$$\begin{bmatrix} X & Y & 1 & 0 & 0 & 0 & -uX & -uY & -u \\ 0 & 0 & 0 & X & Y & 1 & -vX & -vY & -v \end{bmatrix} \begin{bmatrix} h_{11} \\ h_{12} \\ \vdots \\ h_{33} \end{bmatrix} = 0. \tag{9}$$

Eq. (9) is in the form Lx=0, where L is a $2n\times$ 9 matrix. Here, n denotes the point pairs in the model plane and image. At least five independent points for solving Eq. (9) are required. After the determination of the homography matrix, it is possible to find the intrinsic parameters by defining the B matrix as follows:

$$B = A^{-1}A. \tag{10}$$

The B matrix is symmetric. Thus, it is replaced by vector b with six degrees of freedom (DOF):

$$b = \begin{bmatrix} B_{11} & B_{12} & B_{22} & B_{13} & B_{23} & B_{33} \end{bmatrix}. \tag{11}$$

If we assume that h_i is the ith column of H, from Eq. (7) we have:

$$h_i^T B h_j = v_{ij}^T b, \tag{12}$$

$$v_{ij} = [h_{i1}h_{j1}, h_{i1}h_{j2} + h_{i2}h_{j1}, h_{i2}h_{j2}, h_{i3}h_{j1} + h_{i1}h_{j3}, h_{i3}h_{j2} + h_{i2}h_{j3}, h_{i3}h_{j3}]^T. \tag{13}$$

By rewriting Eq. (7) in terms of v:

$$\begin{bmatrix} v_{12}^T \\ (v_{11} - v_{22})^T \end{bmatrix} b = 0. \tag{14}$$

Eq. (14), similar to Eq. (9), is in the form Vb=0, with the difference being that the V matrix has $2n\times$ 6 dimensions, where n is the number of image plane observations. Eq. (9) and Eq. (14) are nonlinear equations that can be solved using metaheuristic methods. After solving Eq. (14), the intrinsic and extrinsic parameters can be obtained as described in the Zhang method [1].

2.4. Lens distortion

Lens distortion is divided into radial and tangential distortions. In many cases, tangential distortion is small and tends to be ignored. However, the first two terms of radial distortions are considered. By assuming (u, v) and (x, y) as the ideal pixel image and normalized ideal pixel image, and (u', v') and (x', y') as the real pixel image and normalized real pixel image, respectively, we have:

$$\begin{cases} u' = u + (u - u_0)[k_1(x^2 + y^2) + k_2(x^2 + y^2)^2] \\ v' = v + (v - v_0)[k_1(x^2 + y^2) + k_2(x^2 + y^2)^2] \end{cases}, \tag{15}$$

where k_1 and k_2 are the desired first two radial lens distortions. Eq. (16) is in the matrix format of Eq. (15). Using n points in m images, we have $2mn$ equations:

$$\begin{bmatrix} (u-u_0)(x^2+y^2) & (u-u_0)(x^2+y^2)^2 \\ (v-v_0)(x^2+y^2) & (v-v_0)(x^2+y^2)^2 \end{bmatrix} \begin{bmatrix} k_1 \\ k_2 \end{bmatrix} = \begin{bmatrix} u'-u \\ v'-v \end{bmatrix}. \tag{16}$$

Eq. (16) is in the form $Dk=d$ and, with matrix manipulation, we can find the k vector as:

$$D^T Dk = D^T d \Rightarrow k = \left(D^T D\right)^{-1} D^T Dd, \tag{17}$$

where T is the matrix transpose operator. In the work of Drap et al. [17], a polynomial model for the calculation of inverse radial lens distortion was presented.

3. Proposed method

Eq. (9) and Eq. (14) are the bottlenecks of the calibration procedure. The accuracy of the solutions may influence the precision of intrinsic, extrinsic, and lens distortion parameters. In this paper, metaheuristic methods are used for optimizing these equations and compared with the SVD method. The proposed method has been examined with four metaheuristic algorithms: the GA [18], PSO [19], colonial competitive algorithm (CCA) [20], and shuffled frog leaping algorithm (SFLA) [21]. Figure 2 shows the block diagram of the proposed algorithm.

As shown in Figure 2, the evolutionary algorithms are used in two steps of the calibration procedure. The stop criteria and cost function of these algorithms are similar to each other. The output of the proposed algorithm is compared with the Zhang method [1] and the numerical SVD solution. The data provided online by Zhang [1] are for researchers to test their algorithms without the influence of edge or corner extraction methods. This reference dataset includes five different views of the checkerboard, five text files of extracted corners corresponding to these images, and finally a text file of the corners of a model checkerboard. The Levenberg–Marquardt (LM) method has been proposed for minimization in the Zhang method [1].

3.1. Cost function

The aim of an evolutionary algorithm is the optimization of a cost function. In this paper, there is a unique cost function for the four proposed metaheuristic algorithms. This function is defined as the mean square of the reprojection error. Both Eq. (9) and Eq. (14) are in the form of the homogeneous equation $Lx=0$. The cost function is defined as follows:

$$error = Lx \Rightarrow Cost = mean(error^2), \tag{18}$$

where x is a vector of nine and six elements in Eq. (9) and Eq. (14), respectively. In each evaluation of the cost function, a matrix of the whole population is assessed. The output of the cost function is a vector of the mean squared error.

3.2. Comparison of methods

The main indicator of calibration precision is the reprojection error. This error can explain to what extent the estimated parameters can correct the distorted captured images towards the ideal model plane. The reprojection

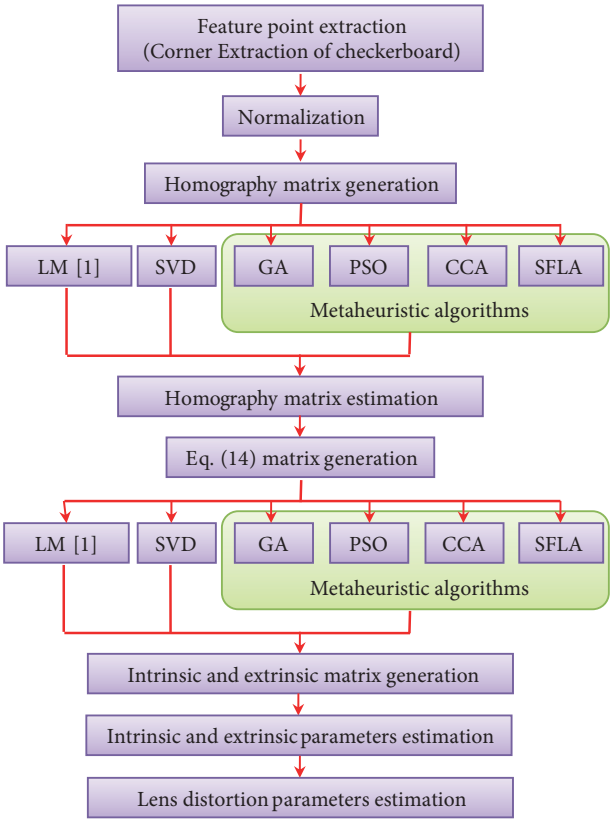

Figure 2. Block diagram of proposed algorithm.

error is defined as follows:

$$reprojection\_error = \left\| \tilde{m} - H\tilde{M} \right\| = \left\| \tilde{m} - A \begin{bmatrix} R & t \end{bmatrix} \tilde{M} \right\|. \tag{19}$$

The average error for each image i is the mean of the reprojection error:

$$average\_error_i = mean\left(\left\| \tilde{m} - H\tilde{M} \right\| \right). \tag{20}$$

The total error is defined as the sum of the average errors over the captured images:

$$total\_error = \sum_{i=1}^{\text{num of images}} average\_error_i. \tag{21}$$

The lens distortions include radial and tangential parameters. In most cases, the tangential parameters are ignored [1], and only the first and second terms of the radial distortions are significant. These two parameters are determined using Eq. (17).

4. Simulation of the dataset

As mentioned in Section 3, the dataset provided in Zhang's paper [1] is used for simulation. The only difference in each simulation is the procedure of parameter estimation. All the simulation results are compared with

unique assessment criteria. The outputs of the numerical and metaheuristic methods are compared with the output of the Zhang method that is provided for researchers [1]. Table 1 shows the simulation results of the proposed method.

Table 1. Intrinsic and lens distortion parameters of dataset of Zhang [1].

		LM [1]	SVD	Metaheuristic algorithms			
				GA	PSO	CCA	SFLA
A	α	832.5	866.0634	882.0014	865.7457	863.5523	860.0798
	β	832.53	866.0468	880.6514	865.7397	863.5448	859.8971
	γ	0.2045	0.1502	0.5298	0.1616	-0.0746	-0.5107
	u_0	303.959	301.1543	295.9408	301.0816	301.4531	296.9451
	v_0	206.585	219.5432	222.0691	219.6324	218.9486	215.8660
k	k_1	-0.228	0.0137	0.0127	0.0137	0.0137	0.0131
	k_2	0.190	-0.0195	-0.0186	-0.0195	-0.0195	-0.0191
Average error of extrinsic parameters	Image 1	2.5702	1.0653	1.4394	1.0632	1.068	1.0527
	Image 2	2.7144	1.0637	1.1677	1.0641	1.0599	1.1182
	Image 3	2.279	1.0192	1.0747	1.0195	1.019	1.1627
	Image 4	2.2053	0.89668	0.90741	0.8971	0.89528	0.9241
	Image 5	1.6671	0.6609	0.66373	0.66068	0.66064	0.66933
Total error		11.4362	4.7058	5.2531	4.7045	4.7027	4.9271

4.1. Smoothness of convergence trace

One the main challenges of using metaheuristic algorithms is the smoothness of the convergence trace. Figures 3 and 4 show the smoothness of the convergence trace for both minimum cost and average cost in the semilogarithmic plot, respectively.

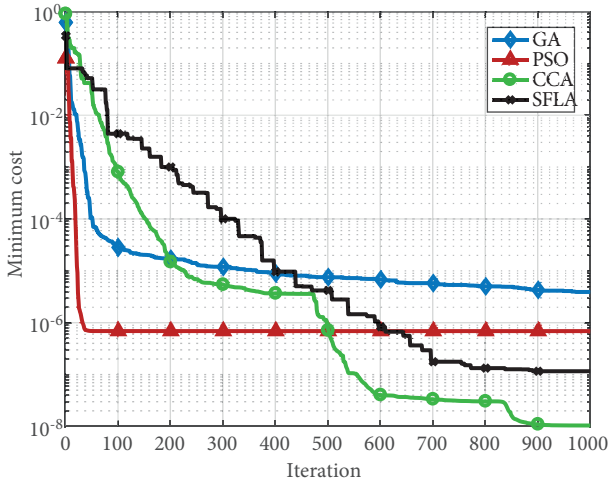

Figure 3. Comparison of convergence trend in homography matrix for estimation for fifth image of dataset.

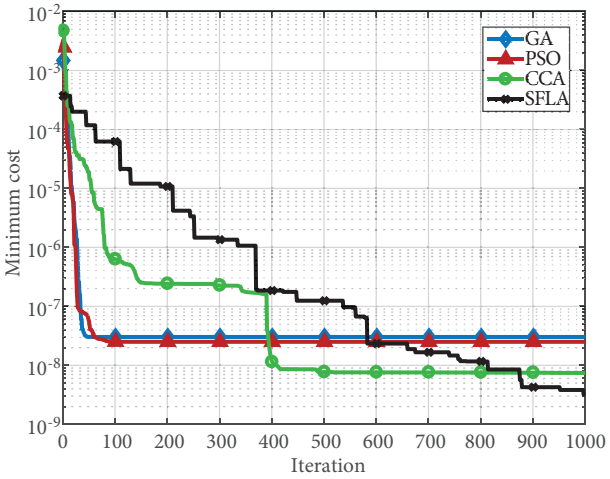

Figure 4. Comparison of convergence trend in Eq. (14) for estimation for fifth image of dataset.

In both Figures 3 and 4, the GA and PSO methods have faster convergence trends than the CCA and the SFLA. By continuing the iteration, there is no significant change in the GA and PSO methods, but the CCA and the SFLA reached better cost function values.

As shown in Figure 4, the minimum cost of the SFLA method is less than that of the CCA method, but the total error of the CCA method is less than that of the SFLA (Table 1). This is due to the effect of the precision of the homography parameter estimation in the previous step, as shown in Figure 5, hierarchically.

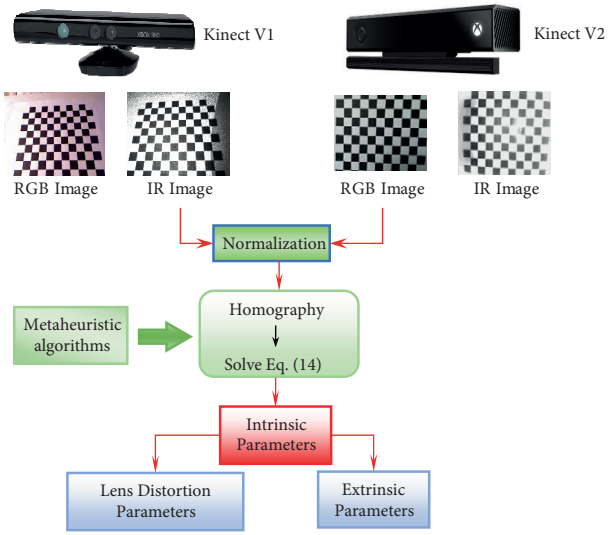

Figure 5. Flow diagram of calibration procedure.

5. Experimental results

In this section, two versions of the Kinect sensor, V1 and V2, are used for the estimation of calibration parameters. Both color and IR cameras are used in this experiment. We show one scene to both cameras of each Kinect sensor and take one snapshot from each camera. Since the IR stream of Kinect V1 is defined in the same RGB stream, it is not possible to take these streams simultaneously. The software program switches between these streams after taking any snapshot from Kinect V1. This problem is solved by the Kinect V2 SDK, and it is possible to take these streams simultaneously.

In both case studies, each Kinect sensor captures eight scenes and tries to fill the whole frame by checkerboard to figure out the lens distortions accurately and precisely. Figures 6 and 7 show images from Kinect V1 and V2, respectively. It should be noted that the color camera of Kinect V2 has a wider width than its IR camera. Moreover, because of the difference in the physical position of the color and IR cameras in both versions of the Kinect sensors, there is a pure translation between the RGB and IR images in each set of snapshots. For the homography estimation, the reprojection error criteria are used as the goal functions that should be minimized by the proposed algorithm.

5.1. Case study 1

In this experiment, Kinect V1 is used for the study. The calibration parameters are compared with the results of Karan [22]. Table 2 shows the calculated values of the calibration parameters. Since the extrinsic parameters depend on the orientation and translation of the checkerboard, these parameters are not compared. Also, in

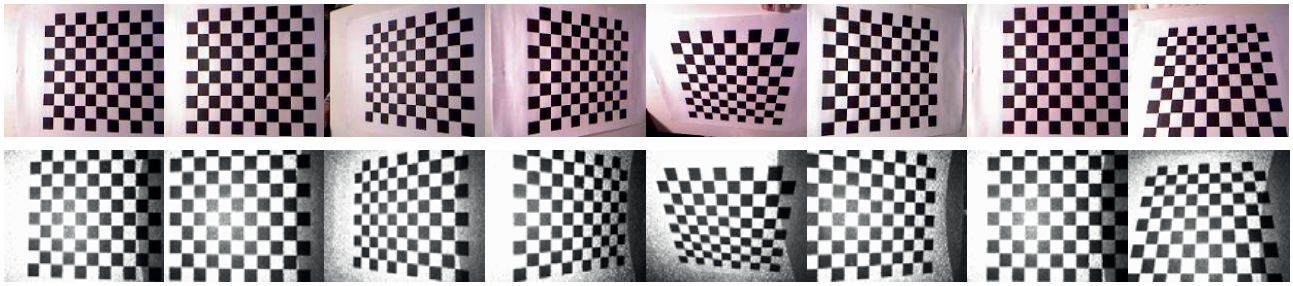

Figure 6. Images captured by Kinect V1: (top) color images, (bottom) IR images.

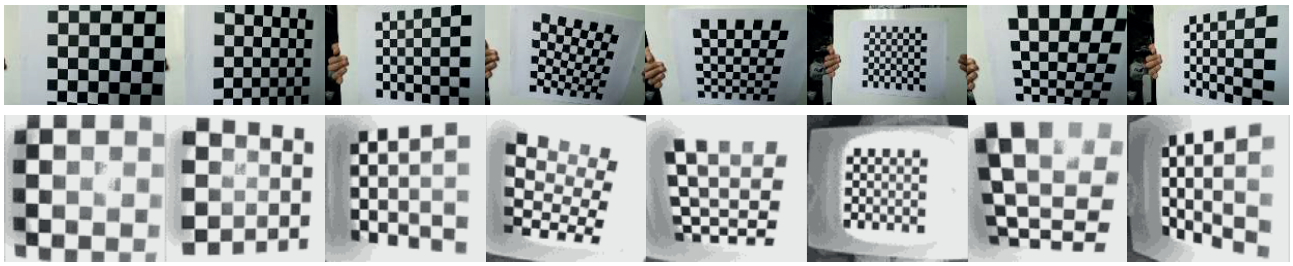

Figure 7. Images captured by Kinect V2: (top) color images, (bottom) IR images.

many cases, the Kinect sensor has various resolutions with different frame speeds. The RGB camera can provide both resolutions of 1280 × 960 at 12 fps and 640 × 480 at 30 fps. The maximum resolution of the IR camera is 640 × 480 at 30 fps. In many applications of this sensor, the 640 × 480 resolution of the RGB camera is therefore used because of the alignment of the depth image and compatibility with the frame speed of the IR camera. The difference of values in lens distortion and other parameters with the same resolution is caused by the manufacturing process. Figure 8 shows the contour map of the radial lens distortion of the Kinect V1 sensor.

5.2. Case study 2

This case study uses Kinect V2 for measuring calibration parameters. The differences between these two versions of Kinect sensors were discussed in a few studies [23]. Table 2 shows the computed calibration parameters of the RGB and IR cameras using the proposed method and compares these parameters with the results of Butkiewicz

Table 2. Intrinsic parameters of proposed method vis-à-vis the results of Karan [22] and Butkiewicz [24].

	Kinect version 1				Kinect version 2			
	RGB	IR	RGB[22]	IR[22]	RGB	IR	RGB[24]	IR[24]
Width	640	640	1280	640	1920	512	1920	512
Height	480	480	960	480	1080	424	1080	424
α	524.0566	588.8036	1043.2	585.5	1065.0149	375.9668	1036.32	364.15
β	522.9802	586.9315	1062.3	586.5	1062.4881	374.2088	1030.40	362.40
u_0	314.0367	317.1854	639.5	327.9	933.1330	255.9834	981.25	250.35
v_0	254.9228	243.2231	479.5	246.2	541.6719	206.5308	523.71	202.89
k_1	0.1498	-0.0759	0.224	-0.125	0.0364	0.0301	0.03451	0.0836
k_2	-0.2691	0.1680	-0.715	0.438	-0.0428	-0.0843	-0.0368	-0.2097

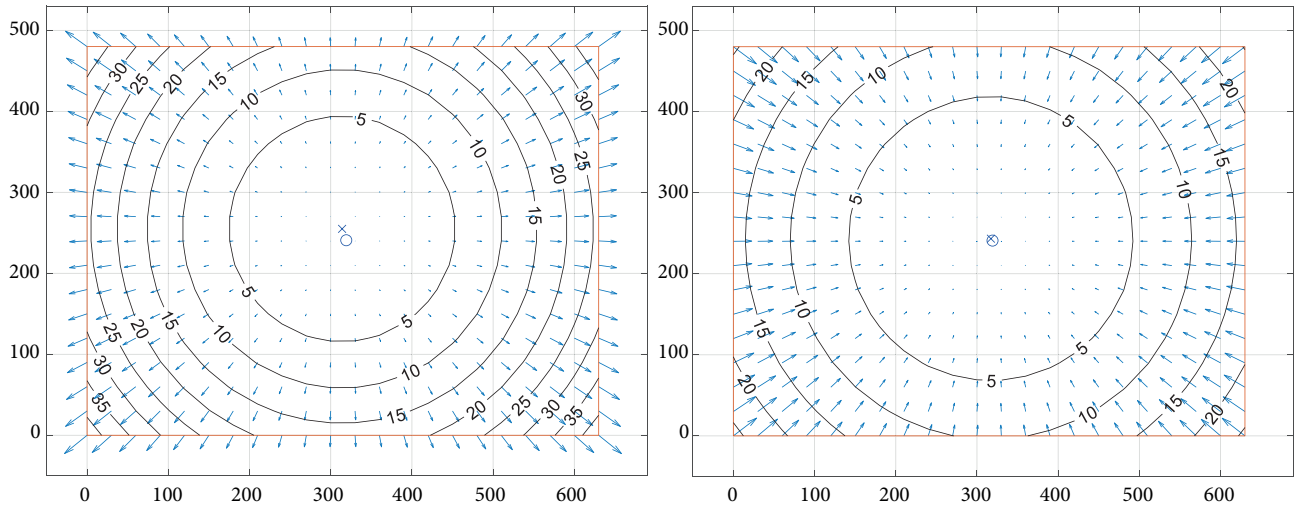

Figure 8. Radial lens distortion of Kinect V1: (left) color camera, (right) IR camera.

[24]. As shown in Figure 9, the RGB camera has a higher resolution with a wider FOV than the IR camera. The IR image does not completely overlap with the RGB image; in many applications, the RGB image should be cropped.

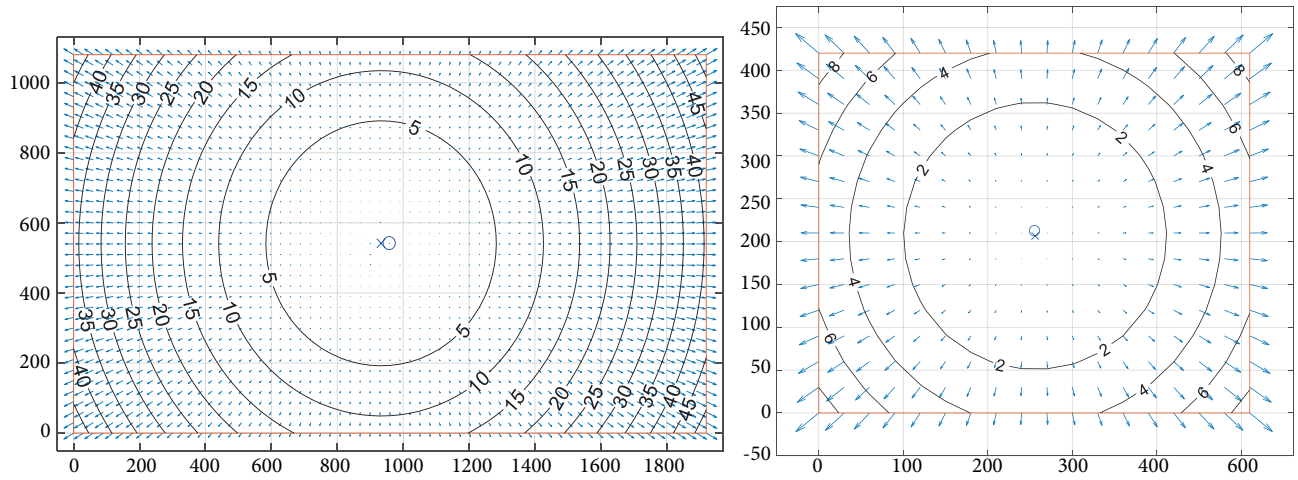

Figure 9. Radial lens distortion of Kinect V2: (left) color camera, (right) IR camera.

5.3. Undistortion

From the values of the lens distortion parameters, it is possible to undistort the captured images as shown in Figures 10 and 11. These outputs may be compared with Figures 6 and 7, respectively. The minority of distortion parameters causes small changes in the undistorted images in comparison to original ones.

6. Conclusion

This paper proposes four metaheuristic algorithms with one numerical method in the camera calibration process. Metaheuristic algorithms are used in two stages of the proposed method, and the accuracy and convergence have improved significantly. We used the GA, PSO, CCA, and SFLA methods in the homography matrix and

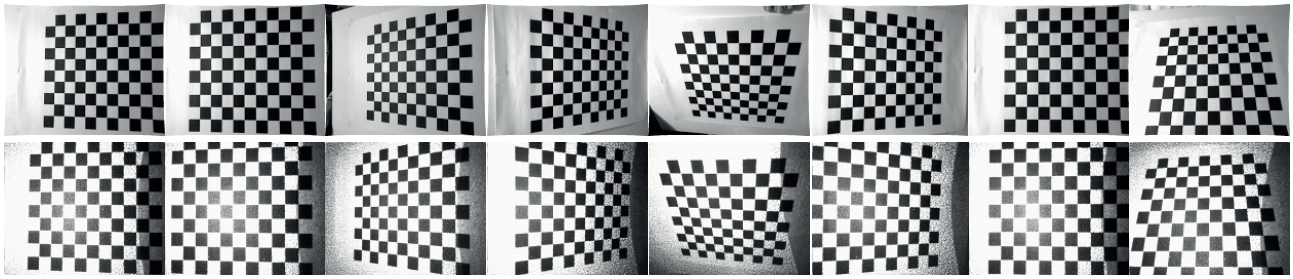

Figure 10. Undistorted Kinect V1: (top) color images, (bottom) IR images.

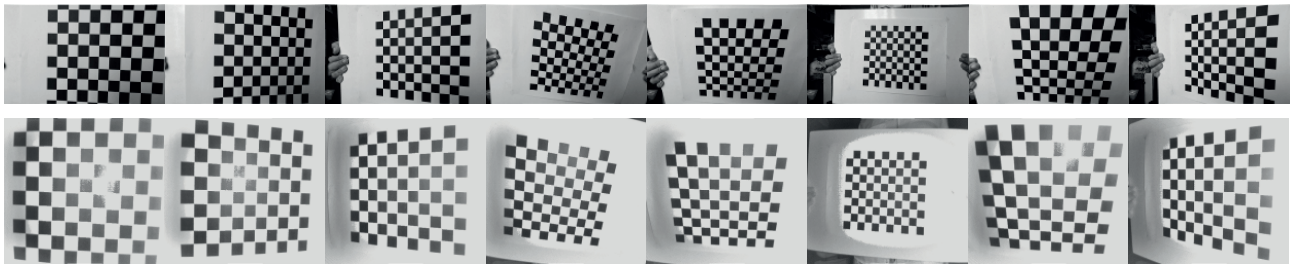

Figure 11. Undistorted Kinect V2: (top) color images, (bottom) IR images.

in the intrinsic and extrinsic parameter estimation. In the simulation results, this paper demonstrates that this method can reduce the total reprojection error criteria in a better way than conventional numerical methods. The experimental results are noted for both versions of Kinect sensors and the outputs are compared with other methods in previous studies. This method is practical, especially in applications where matrix manipulation is time- and power-consuming.

References

[1] Zhang Z. A flexible new technique for camera calibration. IEEE T Pattern Anal 2000; 22: 1330-1334.

[2] Kanatani K. Statistical Optimization for Geometric Computation: Theory and Practice. 1st ed. Amsterdam, the Netherlands: Elsevier, 1996.

[3] Kanatani K, Takeda S. 3-D motion analysis of a planar surface by renormalization. IEICE T Inf Syst 1995; E78-D: 1074-1079.

[4] Kanatani K. Optimal homography computation with a reliability measure. In: IAPR 1998 Workshop on Machine Vision Applications; 17–19 November 1998; Chiba, Japan. pp. 426-429.

[5] Hartley R, Zisserman A. Multiple View Geometry in Computer Vision. 2nd ed. New York, NY, USA: Cambridge University Press, 2004.

[6] Harker MJ, O'Leary PL. Computation of homographies. In: British Machine Vision Conference; 5–8 September 2005; Oxford, UK. pp. 30.1-30.10.

[7] Herrera CD, Kannala J, Heikkila J. Joint depth and color camera calibration with distortion correction. IEEE T Pattern Anal 2012; 34: 2058-2064.

[8] Raposo C, Barreto JP, Nunes U. Fast and accurate calibration of a Kinect sensor. In: IEEE 2013 International Conference on 3D Vision; 29 June–1 July 2013; Seattle, WA, USA. New York, NY, USA: IEEE. pp. 342-349.

[9] Ji Q, Zhang Y. Camera calibration with genetic algorithms. IEEE T Syst Man Cy A 2001; 31: 120-130.

[10] Hati S, Sengupta S. Robust camera parameter estimation using genetic algorithm. Pattern Recogn Lett 2001; 22: 289-298.

[11] Song X, Yang B, Feng Z, Xu T, Zhu D, Jiang Y, Camera calibration based on particle swarm optimization. In: IEEE 2009 2nd International Congress on Image and Signal Processing; 17–19 October 2009; Tianjin, China. New York, NY, USA: IEEE. pp. 1-5.

[12] Merras M, Akkad NE, Saaidi A, Nazih AG, Satori K. Camera self calibration with varying parameters by an unknown three dimensional scene using the improved genetic algorithm. 3D Research 2015; 6: 1-14.

[13] Tsai RY. An efficient and accurate camera calibration technique for 3D machine vision. In: IEEE 1986 Computer Vision and Pattern Recognition Conference; 22–26 June 1986; Miami, FL, USA. New York, NY, USA: IEEE. pp. 364-374.

[14] Yılmaz Ö, Karakuş F. Stereo and Kinect Fusion for continuous 3D reconstruction and visual odometry. Turk J Elec Eng & Comp Sci 2016 24: 2756-2770.

[15] Han J, Shao L, Xu D, Shotton J. Enhanced computer vision with Microsoft kinect sensor: a review. IEEE T Cybern 2013; 43: 1318-1334.

[16] Zhang Z. Camera calibration. In: Medioni G, Kang SB, editors. Emerging Topics in Computer Vision. Upper Saddle River, NJ, USA: Prentice Hall, 2005. pp. 5-44.

[17] Drap P, Lefevre J. An exact formula for calculating inverse radial lens distortions. Sensors 2016; 16: 1-18.

[18] Holland JH. Adaptation in Natural and Artificial Systems. 1st ed. Ann Arbor, MI, USA: University of Michigan Press, 1975.

[19] Kennedy J, Eberhart R. Particle swarm optimization. In: IEEE 1995 Neural Networks International Conference; 27 November–1 December 1995; Perth, Australia. New York, NY, USA: IEEE. pp. 1942-1948.

[20] Atashpaz-Gargari E, Lucas C. Imperialist competitive algorithm: An algorithm for optimization inspired by imperialistic competition. In: IEEE 2007 Evolutionary Computation Congress; 25–28 September 2007; Singapore. New York, NY, USA: IEEE. pp. 4661-4667.

[21] Eusuff M, Lansey K, Pasha F. Shuffled frog-leaping algorithm: a memetic meta-heuristic for discrete optimization. Eng Optimiz 2006; 38: 129-154.

[22] Karan B. Accuracy improvements of consumer-grade 3D sensors for robotic applications. In: IEEE 2013 Intelligent Systems and Informatics Symposium; 26–28 September 2013; Subotica, Serbia. New York, NY, USA: IEEE. pp. 141-146.

[23] Pagliari D, Pinto L. Calibration of Kinect for Xbox One and comparison between the two generations of Microsoft sensors. Sensors 2015; 15: 27569-27589.

[24] Butkiewicz T. Low-cost coastal mapping using Kinect v2 Time-of-flight cameras. In: IEEE 2014 Oceans Conference; 14–19 September 2014; St. John's, Canada. New York, NY, USA: IEEE. pp. 1-9.